Journal of Hydrology 650 (2025) 132490

Contents lists available at ScienceDirect

Journal of Hydrology

journal homepage: www.elsevier.com/locate/jhydrol

Research papers

Spatiotemporal dynamics of global rain-fed groundwater recharge from 2001 to 2020

S. Nazari [a,*], I.L. Kruse [a,b], N. Moosdorf [a,c]

[a] Leibniz Centre for Tropical Marine Research (ZMT), Bremen, Germany
[b] Niels Bohr Institute, University of Copenhagen, Copenhagen, Denmark
[c] Institute of Geosciences, Kiel University, Kiel, Germany

ARTICLE INFO

This manuscript was handled by Emmanouil Anagnostou, Editor-in-Chief, with the assistance of Zoi Dokou, Associate Editor

Keywords:
Global rain-fed groundwater recharge
Global hydrological cycle model
Groundwater stress hotspots

ABSTRACT

Groundwater depletion results from a groundwater withdrawal rate exceeding groundwater recharge. Although groundwater depletion is recognized as a pressing global phenomenon, global groundwater recharge remains one of the least constrained aspects of the global hydrological cycle. This study aims to evaluate the spatial and temporal variations of global rain-fed groundwater recharge over the last two decades (2001–2020), and to assess how climate change and variability have affected the temporal patterns of groundwater recharge. We developed a three-layer transient water balance model to estimate the daily dynamics of global rain-fed groundwater recharge at a spatial resolution of 0.1°. The 20-year average groundwater recharge is estimated to be 176 mm per year. The assessment of the global recharge trend shows that the global groundwater recharge trend has increased by 0.2 mm per year during these 20 years. However, when evaluating the recharge trend of each global river basin, we found that recharge has declined in 40 % of the river basins. These declines are primarily located in South America and Europe, with additional scattered basins in northern Australia and eastern China. In 26 % of the world's basins, declining groundwater storage combined with increasing groundwater recharge, suggests that storage loss is likely due to anthropogenic factors such as over-exploitation, affecting 2.6 billion people. In contrast, in 22 % of basins, the decline in groundwater storage coincides with a decline in groundwater recharge. These basins, inhabited by 1.7 billion people, are climatic hotspots for groundwater sustainability, where drying recharge exacerbates groundwater storage losses.

1. Introduction

Escalating global groundwater depletion has become an urgent concern, with the rate increasing significantly from 56 km^3a^{-1} between 1960 and 2000 to 113 km^3a^{-1} between 2000 and 2009 (Döll et al., 2014b). The alarming trend in the reduction of the largest liquid freshwater resource not only jeopardizes water and food security (Dalin et al., 2017), but also threatens groundwater-dependent ecosystems (de Graaf et al., 2019; Mohan et al., 2023). It also leads to other crises, such as land subsidence, escalating costs associated with groundwater withdrawal, and rising sea levels (United Nations, 2022).

Intensive groundwater withdrawal has historically been identified as the primary factor contributing to groundwater depletion (Dalin et al., 2017; Wada et al., 2014). Increased withdrawal is a consequence of the growing global population (Rodell et al., 2009), improving living standards, and the expansion of industries and agriculture (Alley et al., 2002). Approximately a quarter of the world's freshwater withdrawal is sourced from groundwater resources to meet the basic freshwater demands, including 9 % of industrial, 22 % of domestic, and 69 % of irrigation freshwater consumption (United Nations, 2022).

While groundwater withdrawal is often identified as a critical driver of groundwater depletion, it is important to recognize that depletion occurs when the rate of groundwater withdrawal surpasses the recharge rate (Famiglietti, 2014). Therefore, to evaluate the dynamics of groundwater storage, the role of groundwater recharge needs to be considered. Long-term groundwater recharge trends are influenced by climate change and variability and have impacts on groundwater storage, groundwater quality (Scanlon et al., 2005), and groundwater-dependent ecosystems (Bergkamp and Cross, 2006; Gleeson et al., 2020; Kløve et al., 2011).

Rain-fed groundwater recharge, a vital natural source of groundwater replenishment, is primarily governed by precipitation, total

* Corresponding author.
E-mail address: sara.nazari@leibniz-zmt.de (S. Nazari).

https://doi.org/10.1016/j.jhydrol.2024.132490
Received 19 October 2023; Received in revised form 17 October 2024; Accepted 23 November 2024
Available online 12 December 2024

evapotranspiration, and percolation into the soil layers. The estimation of rain-fed recharge depends on several factors, including soil properties, vegetation types, land use, topography, climate, and the temporal and spatial scales of calculation (Alley et al., 2002; Small, 2005). Due to the scarcity of global-scale recharge observations, calculating recharge from observations or calibrating modeled recharge involves uncertainty and complexity (Moeck et al., 2020b; Wada, 2016).

Global hydrological models (GHMs) and datasets have been used to analyze global groundwater recharge. These studies have primarily focused on simulating long-term average recharge to assess groundwater depletion and water table depth (de Graaf et al., 2017; Döll et al., 2014a; Döll et al., 2014b; Wada et al., 2010), groundwater-surface water interactions (Bierkens et al., 2021; de Graaf et al., 2019), and the impacts of groundwater withdrawal on water resource status (Bierkens et al., 2021; Döll et al., 2012).

Recent studies have investigated rain-fed groundwater recharge (Berghuijs et al., 2022; Jung et al., 2024) and projected the future impacts of climate change on it (Berghuijs et al., 2024; Reinecke et al., 2021). However, comprehensive analyses that quantifys the effects of recent climate change and variability on the temporal variation of rain-fed groundwater recharge—independent of groundwater withdrawals—remain scarce (Kundzewicz et al., 2007). This gap is critical because changes in groundwater recharge trends, whether indicating drying or wetting, significantly impact groundwater management. A drying trend can exacerbate groundwater storage stress, while a wetting trend can help mitigate it (Huggins et al., 2022).

This study aims to evaluate the spatial and temporal variations of global rain-fed groundwater recharge over the past two decades (2001–2020). The primary objective is to assess how climate change and land use variability have influenced the temporal patterns of groundwater recharge. We focus on processes driven mainly by climatic factors, while minimizing the impact of direct anthropogenic influences, except for indirect effects such as those arising from climate or land cover changes. To support this analysis, we developed a grid-based Global Groundwater Rain-fed Recharge (GGR) model.

By utilizing two decades of groundwater storage anomaly data from the Gravity Recovery and Climate Experiment (GRACE) satellite mission (Güntner et al., 2023; Wiese et al., 2016) and an analytical evaluation of how periodic climate variability affects groundwater recharge and water table dynamics (Moeck et al., 2024), we identify regions where recharge variability correlates with groundwater storage fluctuations. Specifically, this study seeks to pinpoint hotspot areas where declining rain-fed recharge exacerbates groundwater storage losses.

For the sake of simplicity, throughout the manuscript, rain-fed groundwater recharge is referred to as 'recharge' and groundwater storage as 'storage'.

2. Methods

2.1. General description

In this study, a grid-based Global Groundwater Rain-fed Recharge (GGR) model utilizing satellite imagery and environmental parameters was developed and implemented in Python (Nazari, 2024). The GGR model operates at a spatial resolution of $0.1^\circ \times 0.1^\circ$ and a daily temporal resolution. The daily temporal resolution was chosen because groundwater recharge is significantly influenced by extreme precipitation events (Berghuijs et al., 2024; Jung et al., 2024) which occur over short periods. Modeling at a daily timescale allows for capturing the impacts of individual rain events on soil moisture dynamics and groundwater recharge processes. The model covers the spatial extent from 180.0°W to 180.0°E longitudes and 60.0°N to 60.0°S latitudes with a temporal range from January 2001 to December 2020.

Based on common definitions of recharge (Gong et al., 2023), in this study, we define it as the water that infiltrates through the evapotranspiration and root zones (Delleur, 2006), penetrates deeply into the soil, and potentially recharges the aquifer (De Vries and Simmers, 2002).

The GGR model consists of three layers: topsoil (root zone), subsoil, and aquifer (Fig. 1), inspired by the approach developed by Hajati et al. (2019). It calculates the exchange of water between the topsoil and atmosphere, as well as surface runoff, water volume in soil layers, subsoil infiltration from topsoil, capillary rise from the subsoil to the topsoil, and groundwater recharge, all on a daily time step and grid-based values.

A different thickness for the layers of each grid was considered based on the absolute depth to the bedrock Z_{total} data (Hengl et al., 2017). The topsoil, subsoil, and aquifer thicknesses Z_{top}, Z_{sub}, and Z_{aq}, respectively, were identified based on Eq. (1):

$$\left(Z_{top}, Z_{sub}, Z_{aq}\right) = \begin{cases} Z_{top} = \mathrm{Z}_{total},\ Z_{sub} = 0, Z_{aq} = 0 & \text{if } \mathrm{Z}_{total} \leq 30 \text{ cm} \\ Z_{top} = 30\mathrm{cm},\ Z_{sub} = \mathrm{Z}_{total} - 30, Z_{aq} = 0 & \text{if } 30 < \mathrm{Z}_{total} \leq 200 \text{ cm} \\ Z_{top} = 30\mathrm{cm},\ Z_{sub} = 170\mathrm{cm}, Z_{aq} = \mathrm{Z}_{total} - 200 & \text{if } \mathrm{Z}_{total} > 200 \text{ cm} \end{cases} \quad (1)$$

The topsoil layer was considered to be up to 30 cm thick to represent the root zone. This layer models the soil-atmosphere interface by incorporating total evapotranspiration and precipitation. The soil moisture capacity of the topsoil layer was used to calculate surface runoff generation in response to precipitation events. The subsoil layer was considered as a transition layer between the topsoil, which is influenced by atmospheric parameters, and the aquifer and can be up to 200 cm in depth. Additionally, the selected thicknesses of the topsoil and subsoil layers were based on the availability of soil data (Simons et al., 2020; Wieder, 2014). This setup leads to neglecting capillary rise from the volume below that threshold, which can lead to an overestimation of recharge.

While the GGR model shares similarities with existing GHMs in calculating rain-fed groundwater recharge, it differs in both its calculation process and the input datasets used. The GGR model incorporates different meteorological and soil properties datasets, and we have reduced the model's complexity and computational demands by omitting the calculation of certain processes (e.g., total evapotranspiration and snowmelt), instead utilizing readily available global datasets.

The default spatial and temporal model setup was determined using meteorological input parameters (Huffman et al., 2019; Muñoz Sabater, 2019). The GGR model begins at 2001, aligned with the available temporal period of the IMERG final run dataset (Huffman et al., 2019) for rainfall. The spatial resolution of 0.1 degrees is dictated by the resolution of the rainfall, total evapotranspiration, and snowmelt datasets. As with other GHMs, uncertainty from the input datasets propagates into our model output (Condon et al., 2021).

Spanning over a 20-year period, this study can capture the effects of some teleconnections that influence groundwater recharge, such as the Pacific-North American (PNA) pattern, the North Atlantic Oscillation (NAO), and the El Niño-Southern Oscillation (ENSO), that typically operate on cycles ranging from 1 to 7 years (Corona et al., 2018; Fleming and Quilty, 2006; Rust et al., 2019). However, longer-term phenomena like the Pacific Decadal Oscillation (PDO), which cycles over 15 to 30 years (Kuss and Gurdak, 2014; Moeck et al., 2024), may not be fully captured within our study period.

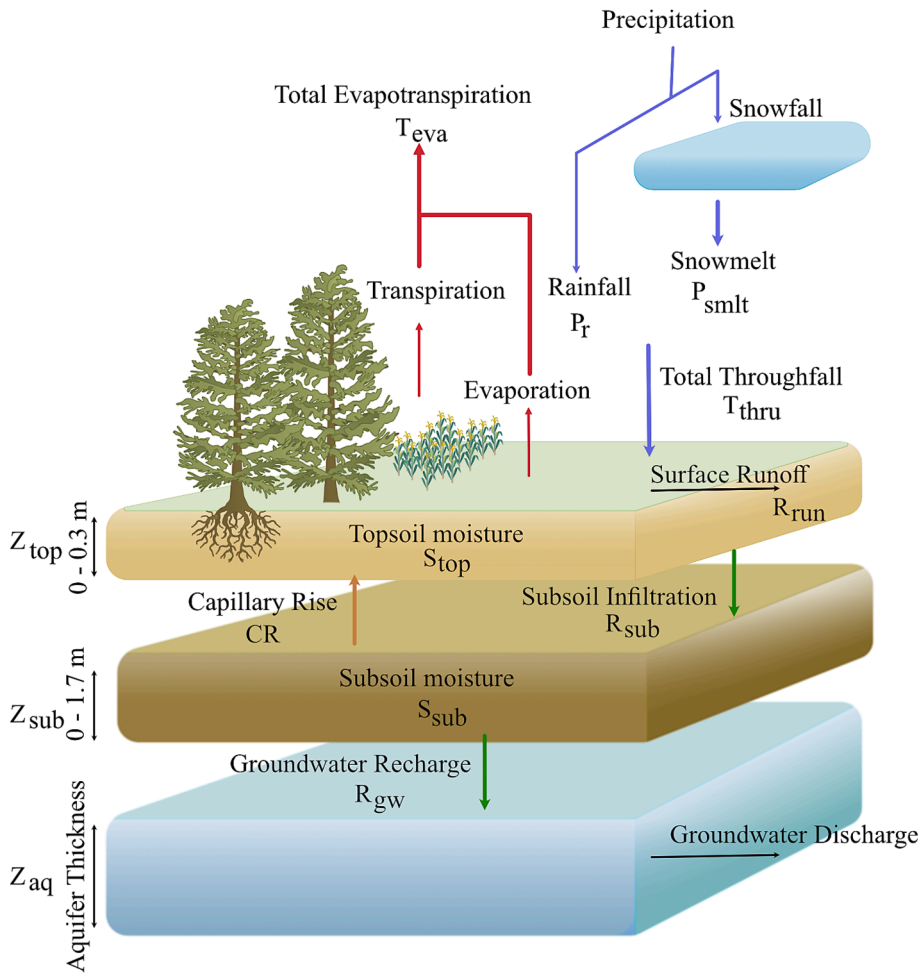

Fig. 1. The conceptual model of the Global Groundwater Rain-fed Recharge (GGR). The diagram illustrates three layers with their respective thicknesses, input meteorological variables, water volumes within soil layers, and the exchanges between the topsoil and atmosphere. It also shows surface runoff, groundwater discharge, and the potential fluxes between soil layers, including capillary rise, subsoil infiltration, and groundwater recharge.

2.2. Input data

Meteorological and soil properties data from various sources were collected as fundamental inputs for the GGR model (see Table 1). These datasets were employed to calculate the interactions between soil and atmosphere, surface runoff, and fluxes within the soil layers, all while accounting the variability of soil composition, land use, and topographical features.

The Integrated Multi-satellite Retrievals for GPM (IMERG) Final Run product (Huffman et al., 2019) was used as the rainfall input data. IMERG Final Run employs sophisticated algorithms to integrate and calibrate various precipitation estimates, ranging from satellite microwave to gauge analysis, at half-hourly resolutions with a spatial scale of 0.1° x 0.1°. Among the different IMERG products, IMERG Final Run is specifically tailored for hydroclimatology and water resources (Li et al., 2021).

The input datasets for snowmelt and total evapotranspiration were sourced from ERA5-Land (Muñoz Sabater, 2019). ERA5-Land is a reanalysis product that provides land-only variables, published by the European Centre for Medium-Range Weather Forecasts (ECMWF), and is available hourly at a spatial scale of 0.1°x0.1°. A land-surface model is used to calculate snowmelt, taking into account factors such as temperature, energy balance, and snowpack properties. ERA5-Land snowmelt represents the amount of melted water from the snow-covered area of a grid. The IMERG Final Run and ERA5-Land datasets were used in conjunction to provide a comprehensive representation of rainfall and snowmelt processes.

Additionally, a combination of meteorological variables, soil properties, and vegetation parameters is used to calculate total evapotranspiration (ECMWF, 2016). ERA5-Land total evapotranspiration is the accumulated amount of water evaporated from the Earth's surface taking into account different components such as low vegetation, high vegetation, and bare soil.

Three sources of soil-related attributes were utilized: SoilGrid250m (Hengl et al., 2017), HiHydroSoil V2.0 (Simons et al., 2020), and HydroPy(v1.0) (Stacke and Hagemann, 2021). SoilGrid250m, provided by the International Soil Reference Information Centre (ISRIC), was used for the total depth to the bedrock input data. This dataset offers predictions of soil properties at seven standard depths and total depth to bedrock. SoilGrid250m employed approximately 150,000 soil profiles in conjunction with remote sensing data, and applied machine learning methods to predict the soil properties across the globe at a resolution of

Table 1
Overview of the input parameters used in the GGR model with the abbreviation (Abbr.), spatial and temporal resolutions (Res.), unit, and source.

Parameter	Abbr.	Res.	Unit	Source
Rainfall	P_r	0.1°(daily)	mm/day	IMERG Final Run, Huffman (2019)
Snowmelt	P_{smlt}	0.1°(daily)	m/day	ERA5, Muñoz Sabater (2019)
Total evapotranspiration	T_{eva}	0.1°(daily)	m/day	ERA5, Muñoz Sabater (2019)
Absolute depth to bedrock	Z_{total}	250 m	cm	SoilGrids250m, Hengl et al. (2017)
Topsoil residual water content	$\theta_{res,top}$	250 m	–	HiHydroSoil v2.0, Simons et al. (2020)
Topsoil saturated water content	$\theta_{sat,top}$	250 m	–	HiHydroSoil v2.0, Simons et al. (2020)
Topsoil unsaturated hydraulic conductivetiy	$K_{f,top}$	250 m	cm/day	HiHydroSoil v2.0, Simons et al. (2020)
Topsoil Alpha parameter for Mualem Van Genuchten Equation	α_{top}	250 m	1/cm	HiHydroSoil v2.0, Simons et al. (2020)
Topsoil N parameter for Mualem Van Genuchten Equation	n_{top}	250 m	–	HiHydroSoil v2.0, Simons et al. (2020)
Subsoil residual water content	$\theta_{res,sub}$	250 m	–	HiHydroSoil v2.0, Simons et al. (2020)
Subsoil saturated water content	$\theta_{sat,sub}$	250 m	–	HiHydroSoil v2.0, Simons et al. (2020)
Subsoil unsaturated hydraulic conductivetiy	$K_{f,sub}$	250 m	cm/day	HiHydroSoil v2.0, Simons et al. (2020)
Subsoil Alpha parameter for Mualem Van Genuchten Equation	α_{sub}	250 m	1/cm	HiHydroSoil v2.0, Simons et al. (2020)
Subsoil N parameter for Mualem Van Genuchten Equation	n_{sub}	250 m	–	HiHydroSoil v2.0, Simons et al. (2020)
Sub-grid distribution parameter	b_{sg}	0.5°	–	HydroPy(v1.0), Hagemann and Gates (2003)Stacke and Hagemann (2021),
Orographical sub-grid standard deviation	σ_h	0.5°	m	HydroPy(v1.0), Amante and Eakins (2009)Stacke and Hagemann (2021),

250 m (Hengl et al., 2017).

For soil hydraulic properties, HiHydroSoil V2.0 was used. HiHydroSoil implements soil properties based on SoilGrid250m and pedotransfer functions to evaluate global soil hydraulic properties on 250 m resolution for six standard depths, as well as topsoil and subsoil layers (Simons et al., 2020). Furthermore, two soil-related datasets were obtained from a data repository provided by HydroPy model, a global hydrological model with a resolution of 0.5° (Stacke and Hagemann, 2021).

While these datasets were globally available, they vary in temporal or spatial resolutions (refer to Table 1). To ensure consistency, all input data were considered daily and were adjusted to a spatial resolution of 0.1° × 0.1°. Input data with a resolution of 250 m were reprojected to a geographical coordinate system and aggregated to 0.1° using averages.

2.3. Model structure

GGR simulates daily transient water balances per cell over three layers. The model estimates changes in the daily amount of topsoil water, S_{top}(t) (mm), based on total throughfall into the ground and total evapotranspiration. The topsoil layer is replenished by total throughfall T_{thru}(t) (mm/day) and capillary rise from subsoil CR(t) (mm/day), while it losses water through total evapotranspiration T_{eva}(t) (mm/day), subsoil infiltration R_{sub}(t) (mm/day), and surface runoff R_{run}(t) (mm/day) (Eqs. (2) and (3)).

$$T_{thru}(t) = P_r(t) + P_{smlt}(t) \tag{2}$$

$$S_{top}(t+\Delta t) = S_{top}(t) + T_{thru}(t) + CR(t) - T_{eva}(t) - R_{run}(t) - R_{sub}(t) \tag{3}$$

where P_{smlt}(t) (mm/day), and P_r(t) (mm/day) are snowmelt, and rainfall, respectively.

The subsoil water volume S_{sub}(t) (mm) is influenced by recharge from topsoil R_{sub}(t) and discharge resulting from groundwater recharge R_{gw}(t) (mm/day), along with capillary rise CR(t) from the subsoil to the topsoil (Eq. (4)).

$$S_{sub}(t+\Delta t) = S_{sub}(t) + R_{sub}(t) - R_{gw}(t) - CR(t) \tag{4}$$

The calculation of the daily recharge for every grid point involves a series of flux estimations. The specific steps of this calculation sequence are outlined in Fig. 2, describing the usage of the input data and the equations explained in the following sections.

2.4. Surface runoff and vertical fluxes simulation

The available topsoil water volume S_{top}(t) and soil properties determine the proportion of total throughfall T_{thru}(t) turning into surface runoff R_{run}(t). In the GGR model, the Improved Arno scheme (IA scheme) (Hagemann and Gates, 2003) was applied to simulate R_{run}(t). The IA scheme assumes a bucket-type reservoir and estimates the excess infiltration as surface runoff in response to the fraction of the topsoil saturation. When the topsoil layer is not saturated, T_{thru} infiltrates and no surface runoff occurs. However, when the soil is saturated, the fraction of soil moisture determines the fraction of T_{thru} changing to R_{run}. The IA scheme applies a shape parameter b (−) and maximum and minimum soil water volume capacities, $S_{max,top}$ (mm) and $S_{min,top}$ (mm), respectively, to account for topsoil moisture variability and calculate surface runoff (Eq. (6)).

The shape parameter b is derived based on the distribution parameter b_{sg} (−) and the sub-grid orography standard deviation σ_h (m), as shown in Eq. (5), to consider how the distribution of the soil moisture affects surface runoff.

$$b = \begin{cases} b_{sg} + b_{oro} & \text{if } b_{oro} > 0.01 \\ b_{sg} & \text{otherwise}, \end{cases} \tag{5}$$

$$R_{run}(t) = \begin{cases} 0 & T_{thru}(t) < S_{top}(t) - S_{min,top} \\ T_{thru}(t) - \left(S_{max,top} - S_{top}(t)\right) + & \\ S_{dif,top} \cdot \left(x^{\frac{1}{b+1}} - \dfrac{T_{thru}(t)}{(b+1)S_{dif,top}} \right)^{b+1} & S_{top}(t) - S_{min,top} \le T_{thru}(t) < (b+1)S_{dif,top}x^{\frac{1}{b+1}} \\ T_{thru}(t) - \left(S_{max,top} - S_{top}(t)\right) & T_{thru}(t) \ge (b+1)S_{dif,top}x^{\frac{1}{b+1}} \end{cases} \quad (6)$$

where $b_{oro} = \frac{\sigma_h - \sigma_0}{\sigma_h + \sigma_{max}}$ and σ_0 and σ_{max} are the minimum and maximum of the standard deviation of the sub-grid orography and equal to 100 m and 1000 m, respectively.

Maximum topsoil water volume capacity $S_{max,top}$ and minimum topsoil water volume capacity $S_{min,top}$ are calculated as functions of the saturated water content $\theta_{sat,top}$ (−), residual water content $\theta_{res,top}$ (−), and topsoil thickness Z_{top} (mm); hence, $S_{max,top} = \left(\theta_{sat,top} - \theta_{res,top}\right) \times Z_{top}$ and $S_{min,top} = \theta_{res,top} \times Z_{top}$. In addition, $S_{dif,top}$ (mm) equals to the differences of $S_{max,top}$ and $S_{min,top}$, and x (−) is calculated as a fraction of the available topsoil layer moisture to this difference ($x = \frac{S_{max,top} - S_{top}(t)}{S_{dif,top}}$).

The next step in the GGR calculation procedure is to determine subsoil infiltration R_{sub}(t) as equal to the unsaturated topsoil hydraulic conductivity K_{top}(t) (mm/day) based on Eq. (8); hence, $R_{sub}(t) = K_{top}(t)$.

The Mualem Van Genuchten equation was applied to estimate the unsaturated hydraulic conductivity (Van Genuchten, 1980). Based on Mualem's model (Mualem, 1976), Van Genuchten (1980) described a simple equation to calculate the unsaturated hydraulic conductivity, containing a pressure head and three independent curve fitting

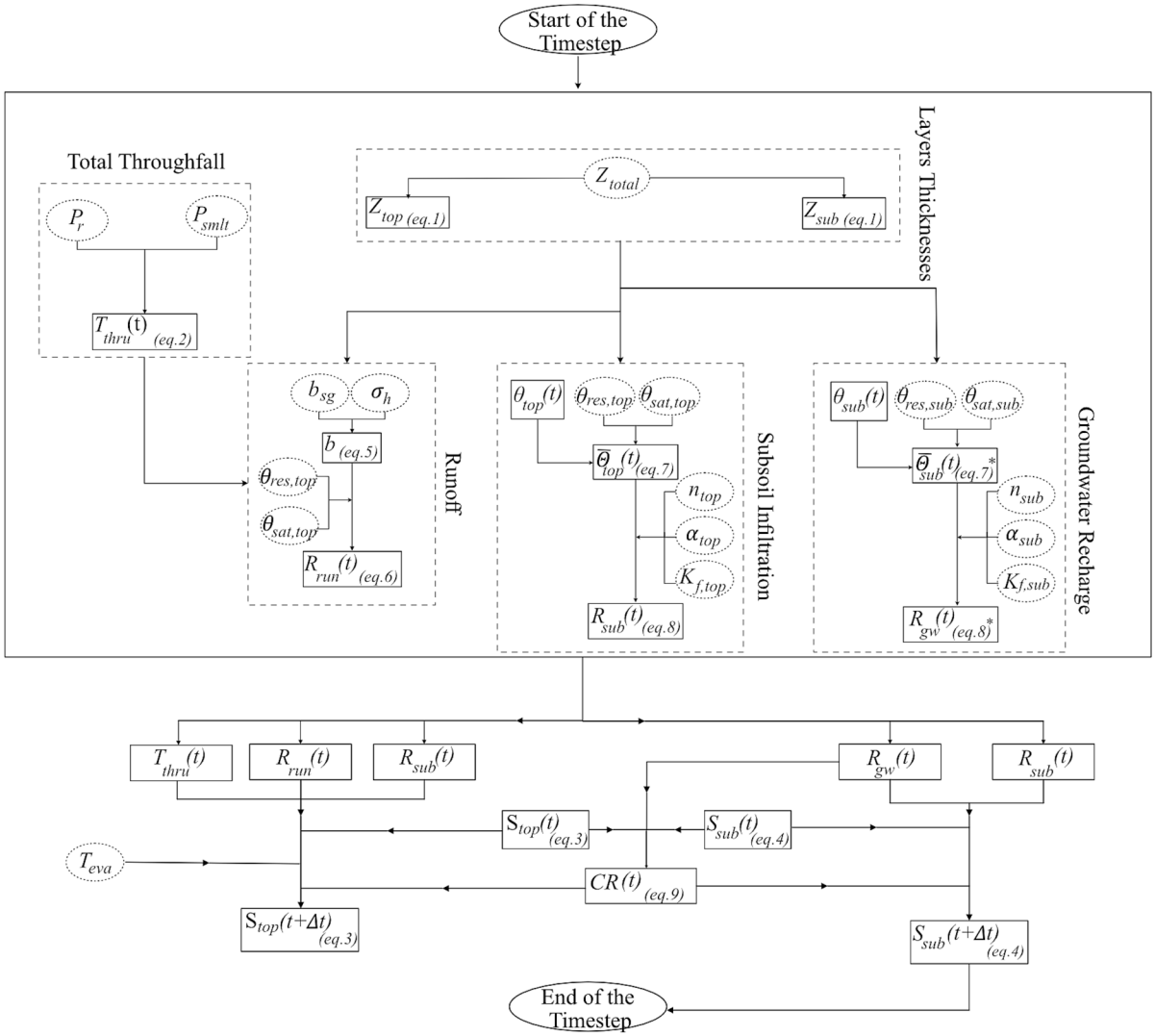

Fig. 2. A flowchart of the sequence of calculations in the GGR model needs to be performed to estimate rain-fed groundwater recharge, including the input parameters and equations described in the method section. $\theta_{top}(t)$ and $\theta_{sub}(t)$ are calculated as a ratio of S_{top}(t) and S_{sub}(t) to the total volume of the topsoil and subsoil, respectively.* equation (7) and (8) are also used for calculating groundwater recharge like subsoil infiltration with the application of the subsoil properties.

parameters. The pressure head h_{top}(t) was estimated as a function of effective saturation $\overline{\Theta}_{top}$(t) based on Eq. (7).

$$\overline{\Theta}_{top}(t) = \frac{\theta_{top}(t) - \theta_{res,top}}{\theta_{sat,top} - \theta_{res,top}} = \left[1 + (\alpha_{top} h_{top}(t))^{n_{top}}\right]^{-m_{top}} \quad (7)$$

$$K_{top}(t) = K_{f,top}\overline{\Theta}_{top}(t)^{0.5}\left(1 - \left[1 - \overline{\Theta}_{top}(t)^{\frac{1}{m}}\right]^{m}\right)^{2} \quad (8)$$

The parameter $K_{f,top}$ (mm/day) represents the saturated hydraulic conductivity. Moreover, α_{top} (mm^{-1}) and n_{top} (−) are the Mualem Van Genuchten curve-fitting parameters of the topsoil, which present the soil water retention curve and are derived empirically, and $m_{top} = 1 - 1/n_{top}$. The available water content in the topsoil at time step t represented by θ_{top}(t) (−) is a ratio of S_{top}(t) to the total volume of the topsoil.

In order to estimate the subsoil water volume, subsoil infiltration from the topsoil R_{sub}(t), recharge R_{gw}(t), and capillary rise CR(t) values are required. Similar to subsoil infiltration (Eqs. (7) and (8)), R_{gw}(t) is determined by subsoil unsaturated hydraulic conductivity K_{sub}(t) (mm/day). Moreover, the capillary rise from the subsoil to topsoil CR(t) is a function of the topsoil water content S_{top}(t) and subsoil unsaturated hydraulic conductivity K_{sub}(t) (Eq. (9)).

$$CR(t) = \begin{cases} K_{sub}(t)\overline{\Theta}_{sub}(t)(1 - \overline{\Theta}_{top}(t)) & \overline{\Theta}_{sub} > \overline{\Theta}_{top} \\ 0 & \overline{\Theta}_{sub} \le \overline{\Theta}_{top} \end{cases} \quad (9)$$

Once the soil layers' water volume is computed, it is checked to stay within the maximum water storage capacities. Accordingly, when $S_{sub}(t + \Delta t)$ exceeds $S_{max,sub}$, it is assumed $S_{sub}(t + \Delta t) = S_{max,sub}$ and the surplus is added to the topsoil water storage and if $S_{top}(t + \Delta t) > S_{max,top}$, the topsoil water storage is considered as $S_{max,top}$ and the difference is added to the surface runoff.

2.5. Spatial aggregation

To estimate recharge and other fluxes at the global river basin scale, the HydroBASINS dataset was utilized (Lehner and Grill, 2013). This dataset provides the river basin areas at various levels, ranging from large basins at level 1 representing each continent to finer basins at level 12. HydroBASINS level 4 was used here. The zonal statistics method of the rasterstats Python module (https://github.com/perrygeo/python-rasterstats) was employed to evaluate the average flux values for each river basin.

2.6. Groundwater storage variations

To investigate the potential impact of recharge dynamics on storage variability, we used the Global Gravity-based Groundwater Product (G3P) (Güntner et al., 2023). G3P is a distinctive dataset derived from observations made by the Gravity Recovery and Climate Experiment (GRACE) satellite mission and GRACE Follow-On (GRACE-FO) (Wiese et al., 2016). The GRACE satellite mission stands out as the sole remote sensing technology capable of monitoring subsurface mass variations. GRACE provides a global dataset of monthly gravity anomalies that reflect changes in total Terrestrial Water Storage (TWS) (Chen et al., 2016; Humphrey et al., 2023; Rodell et al., 2018).

TWS anomalies encompass variations in multiple storage components, including groundwater, surface water, soil moisture, glacier, and snow. G3P was developed using a mass balance approach to exclusively represent the Groundwater Storage Anomaly (GWSA) data (Sharifi and Güntner, 2022). Evaluations of in-situ groundwater observations for 13

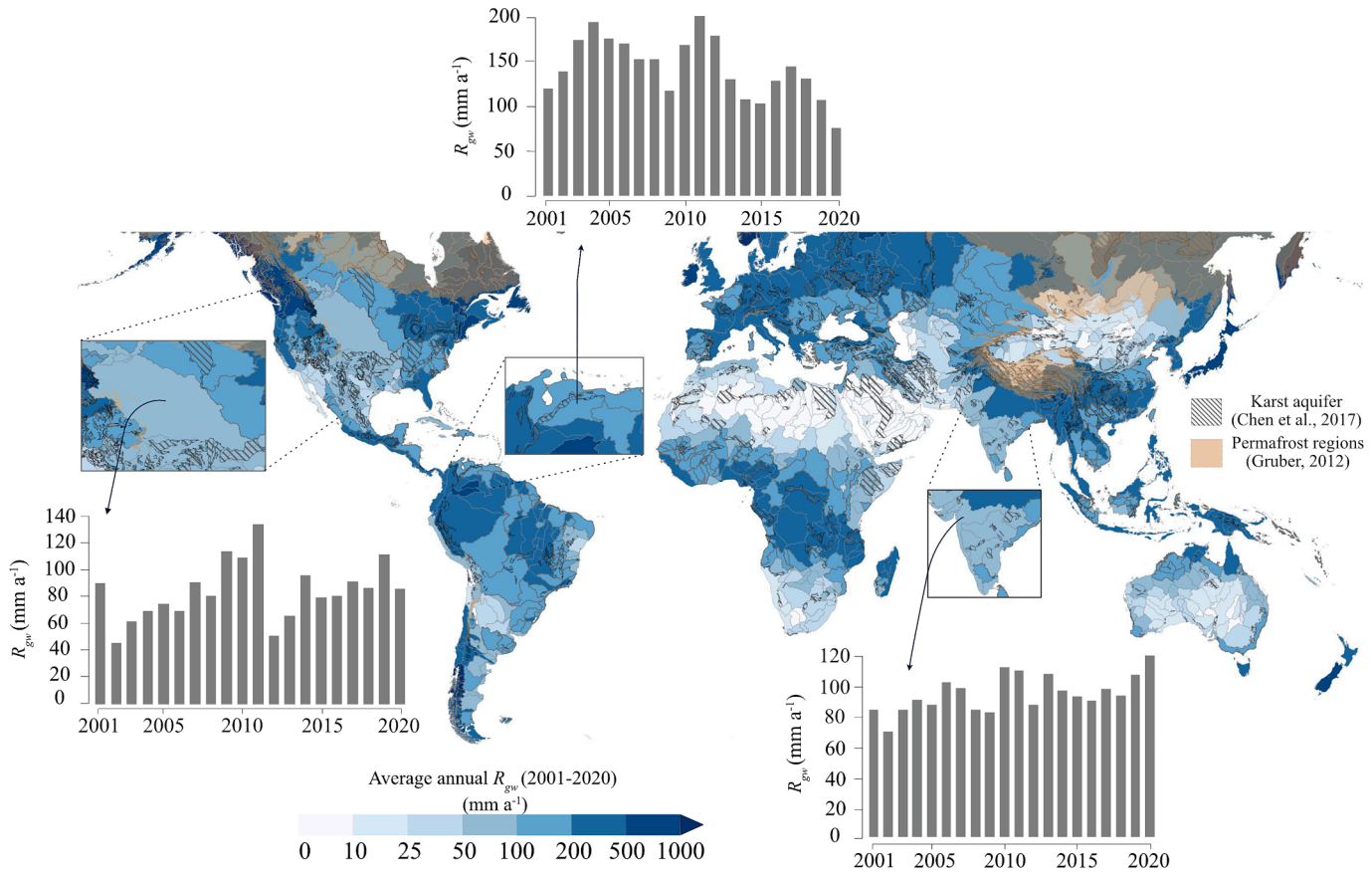

Fig. 3. Average rain-fed groundwater recharge for each basin from 2001 to 2020. Bar charts of three sample basins exemplify the underlying annual rain-fed groundwater recharge. Permafrost and karstic areas are highlighted because of increased uncertainty of the results in these areas.

large basins worldwide showed a high correlation between the GWSA and the variations in groundwater observations (Sharifi et al., 2023). G3P provides information from 2002 to the present, with monthly temporal resolution and a spatial resolution of 0.5°, covering the entire globe.

In this study, we applied G3P to calculate temporal variations in storage. For each grid point, we computed the temporal trend in storage by conducting a linear regression on the GWSA time series within the 2002–2020 time window and extracting the slope. This quantity was defined as the groundwater storage anomaly (GWSA) trend.

Due to the long groundwater system response times (Cuthbert et al., 2019), we assume that alterations in discharge pattern from a groundwater body exhibit a temporal lag in response to changes in recharge dynamics. Therefore, significant shifts in recharge rates are expected to be detected in a trend calculated from GWSA over a period of 19 years that could be detected in the G3P.

Uncertainty in the G3P product can be attributed to several factors, including satellite measurement errors, soil moisture and snow water equivalent corrections, and groundwater-surface water partitioning. Although there are uncertainties in the G3P, the product has shown higher correlation with in situ groundwater data at the large aquifer scale than at the pixel level. This is because large aquifer dynamics are better captured by satellite measurements, whereas pixel-based assessments require more detailed assessment of water compartments, which increases uncertainty (Vinueza et al., 2023).

The declining trend of GWSA was considered a significant indicator of storage loss and stressed groundwater basins. The GWSA trend was utilized to evaluate its co-occurrence with the recharge trend, helping to detect the role of recharge on storage dynamics. This analysis also facilitated the identification of hotspot areas experiencing sinking storage and declining recharge.

In addition, to assess the extent to which recharge trends influence groundwater storage, we incorporated annual (365 days) and decadal (3652 days) damping depths, following the methodology outlined by Moeck et al. (2024). Damping depth is defined as the depth below the surface where only 5 % of the flux variation is preserved, reflecting the extent to which the unsaturated zone dampens infiltration signals. This is influenced by factors such as soil properties, the timescale of flux variations, and average recharge rates (Dickinson et al., 2014; Moeck et al., 2024). By distinguishing between transient and steady-state recharge behavior over different periodic cycles, this approach enables us to capture how recharge signals propagate through the vadose zone and identify regions where groundwater storage is more sensitive to climate-driven recharge variability.

Specifically, we calculated the damping depth for both annual (365 days) and decadal (3,652 days) periods and evaluated whether recharge

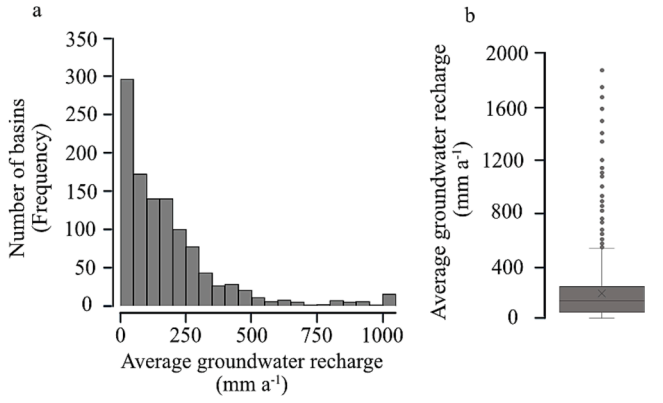

Fig. 4. Average annual rain-fed groundwater recharge per basin unit statistics (a) frequency histogram of average recharge per basin; and (b) box plot of river basin recharge presenting interquartile ranges, median, and mean values, respectively.

Table 2
Comparison between global groundwater recharge estimations of various models, including this study, and observed groundwater recharge.

Approach	S. Res.	T. Res.	Timespan	R_{gw} (mm a^{-1})	R^2	Source
WaterGAP 2	0.5°	Daily	1960–2001	107	0.26[a]	Döll and Fiedler (2008)
PCR-GLOBWB	0.1°	Daily	1957–2002	111	0.26[a]	de Graaf et al. (2015)
PCR-GLOBWB	0.1°	Daily	1960–2010	121	0.19[a]	de Graaf et al. (2019)
WaterGAP v2. 2d	0.1°	Daily	1901–2016	141	0.46[a]	Müller Schmied et al. (2021)
Sigmoid Function	0.008°[b]	–	1968–2018	218	0.41[a]	Berghuijs et al. (2022)
GGR	0.1°	Daily	2001–2020	160	0.41	

[a] R^2 is presented based on the Berghuijs et al. (2022) study that compares each study's modeled global groundwater recharge with observations.
[b] The spatial resolution of this recharge is presented based on the published data (Berghuijs, 2022).

in each basin behaves in a transient or steady-state manner over these timescales. In river basins where recharge is classified as transient at either the annual or decadal scale, we expect to observe the impact of recharge variability on groundwater storage. This assessment was conducted by analyzing the majority of grid values within each basin to determine if recharge is dampened by the vadose zone or if it remains transient, indicating more influence on groundwater storage.

3. Results and discussion

3.1. Spatial distribution of global recharge

According to the model, the average global groundwater recharge is 176 mm a^{-1} over the period from 2001 to 2020 (Fig. 3), with a median value of 120 mm a^{-1}. The spatial distribution of R_{gw} closely mirrors the precipitation patterns. The 25th percentile of grid cells (R_{gw} < 36 mm a^{-1}) is concentrated in arid regions, such as the Sahara Desert, Saudi Arabia, Yemen, and Oman, as well as some basins in Iraq, Iran, China, and southern Africa. In contrast, the 75th percentile (R_{gw} > 241 mm a^{-1}) of grid cells is found in tropical and northern mid-latitude regions, e.g., in Europe, North America, and the Himalayas.

Since the GGR model does not account for permafrost processes or the macropore flow characteristic of karstic aquifers, regions with permafrost (Gleeson et al., 2014; Gruber, 2012) and karstic aquifers (Chen et al., 2017) are highlighted in Fig. 3. Recharge estimates in these regions may be subject to additional uncertainty because the model is unable to capture the specific hydrological processes operating in these unique geological settings.

The range of R_{gw} spans from 0 mm a^{-1} to 1876 mm a^{-1} on average per basin (Fig. 4b). The frequency distribution of R_{gw} reveals that 27 % of basins experience an average recharge of less than 50 mm a^{-1} (Fig. 4a). In contrast, for 6 % of the river basins, R_{gw} exceeds 500 mm a^{-1}, predominantly located in North America. Nearly half (48 %) of the population residing within the latitudes of 60°S to 60°N in 2020 (Center for International Earth Science Information Network - CIESIN - Columbia University, 2018), live in basins with recharge below the global average.

3.2. Global recharge comparison

GHMs that estimate groundwater recharge are often evaluated using proxies such as streamflow observations rather than groundwater recharge measurements (Berghuijs et al., 2022). In this study, we compared the GGR model results with both global groundwater recharge

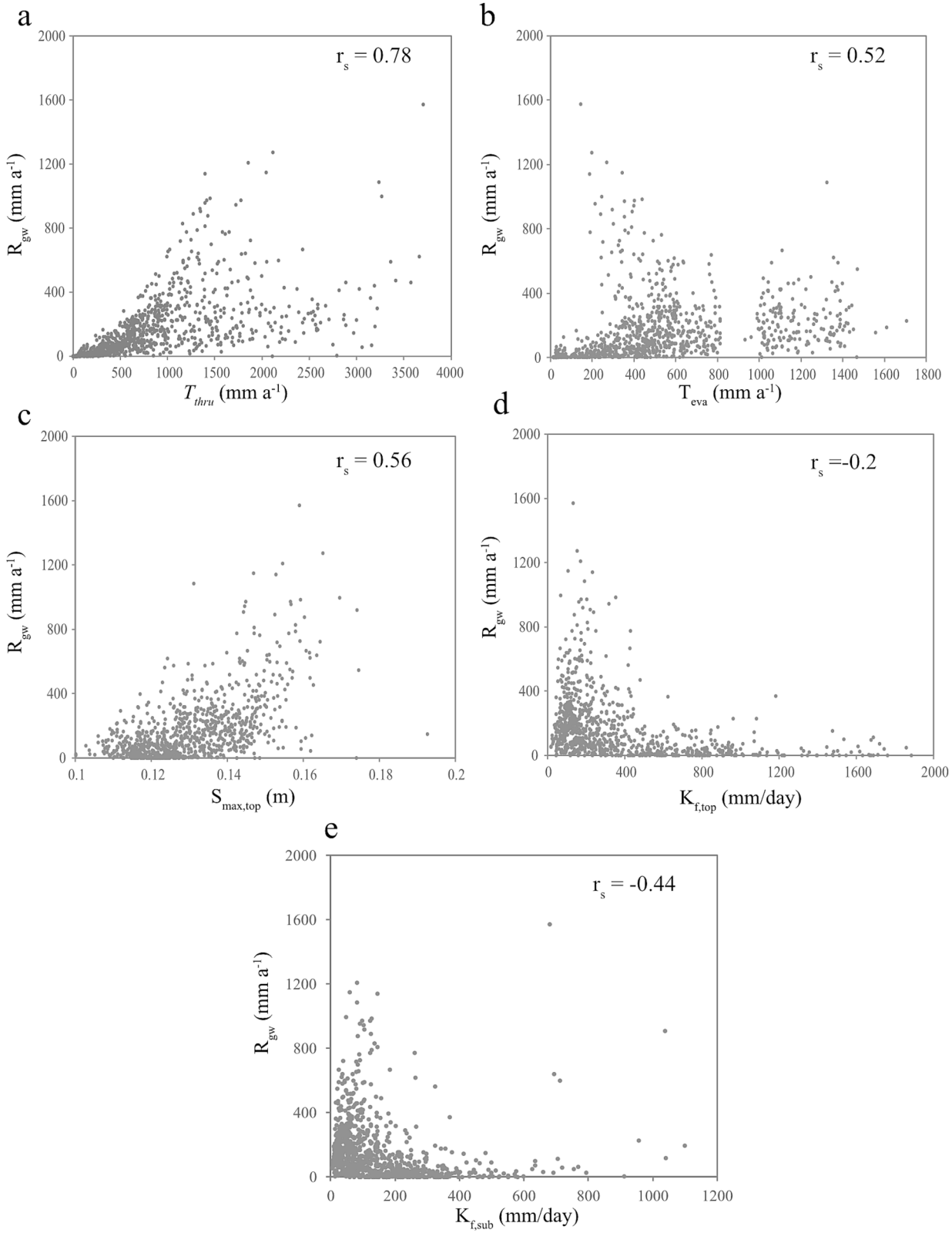

Fig. 5. Spearman's Rho correlation r_s assessment between groundwater recharge R_{gw} and five input variables (a) total throughfall T_{thru}; (b) total evapotranspiration T_{eva}; (c) topsoil maximum water storage capacity $S_{max,top}$; (d) topsoil saturated hydraulic conductivity $K_{f,top}$; and (e) subsoil saturated hydraulic conductivity $K_{f,sub}$.

estimates from previous studies (Berghuijs et al., 2022; de Graaf et al., 2019; de Graaf et al., 2015; Döll and Fiedler, 2008; Müller Schmied et al., 2021; Simon N. Gosling et al., 2024) and global recharge measurement datasets (Moeck et al., 2020a).

While the GGR model exhibits a similar spatial distribution of recharge to other global estimations, differences in recharge estimates are particularly pronounced in certain regions (Fig. SF3). For example, in tropical areas such as Indonesia, the GGR model estimates lower

recharge values compared to other models, while in arid and semi-arid regions like the Sahara and parts of Australia, it predicts higher recharge rates.

When comparing the R_{gw} with global recharge measurement points, the R^2 value of the GGR model is 0.41, placing it among the most favourable models in terms of performance (Table 2, Fig. SF4). Across all measurement points, 16 % of the GGR model's long-term average annual recharge estimates fall within 30 % of the observed values, while 38 % are within 50 % (Fig. SF5). The GGR model generally provides results closer to the observations than the compared long-term recharge estimates, with the exception of the empirical sigmoid function (Berghuijs et al., 2024; Berghuijs et al., 2022), which performs better.

Overall, the GGR model tends to overestimate recharge, particularly in Australia, where a significant portion of the measurement points are located. Wan et al. (2024) similarly found that the WaterGAP2.2e model overestimated recharge in Australia, which they attributed to native vegetation not being accurately represented in the model's land cover data, as it relies on the MODIS dataset. Likewise, the GGR model uses total evapotranspiration data from ERA5-Land (Muñoz Sabater, 2019), which also incorporates MODIS land cover data. This likely contributes to the overestimation of recharge in these regions. Thus, improving land cover classification and the associated evapotranspiration parameters in input data will likely improve recharge estimates of the GGR and similar models.

The correlation between modeled recharge and observations are generally modest, largely due to the uncertainties associated with both the modeled recharge and the measurement data. These uncertainties arise from differences in modeling approaches, the global scale input datasets, observation techniques, and limitations in the availability of global in-situ data. Additionally, the temporal mismatch between observation periods and modeled recharge estimates, combined with the uneven spatial coverage of observation points, makes it challenging to more accurately evaluate the performance of the modeled groundwater recharge.

3.3. Controls on recharge

To evaluate the sensitivity of R_{gw} to input parameters, we conducted Spearman's Rho correlation r_s analysis. The selected input variables include the total throughfall T_{thru}, total evapotranspiration T_{eva}, topsoil maximum water storage capacity $S_{max,top}$, topsoil saturated hydraulic conductivity $K_{f,top}$, and subsoil saturated hydraulic conductivity $K_{f,sub}$. A total of 1000 sample points were randomly selected worldwide, and the correlation between groundwater recharge and each of these variables based on the grid unit was determined.

The strongest correlation is observed between total throughfall and recharge, with a correlation coefficient of 0.78 (Fig. 5a). However, high precipitation does not always create higher recharge values, e.g., when soil layers are saturated or rainfall events are too intense for percolation

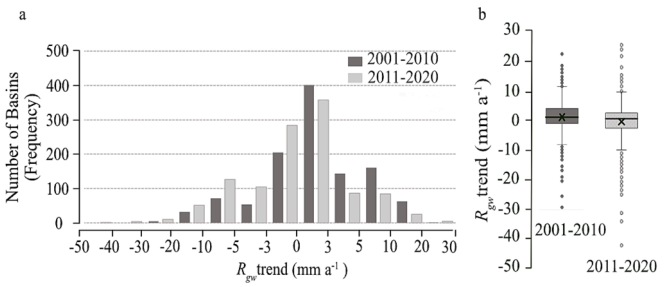

Fig. 7. Average annual rain-fed groundwater recharge R_{gw} trend per basin unit statistics (a) frequency histogram of recharge trend per basin from 2001–2010 and 2011–2020; and (b) comparison of recharge trend box plots presenting the interquartile ranges for each ten-year trend assessment separately. The black line and × show the median and the mean values, respectively.

to generate R_{gw}. Additionally, soil properties can play a role, as high rainfall amounts often occur in areas with lower hydraulic conductivities, inhibiting their recharge effect (Supplementary Fig. SF1).

Total evapotranspiration correlates positively with R_{gw} (r_s = 0.52, Fig. 5b). This study accounts for land cover and vegetation types through the total evapotranspiration data. Therefore, high total evapotranspiration occur in areas with high precipitation (r_s = 0.86, calculated between precipitation and total evapotranspiration, Supplementary Fig. SF1). It is evident that total evapotranspiration exceeding 1000 mm a^{-1} primarily occurs in tropical areas, whereas the range of 800 < T_{eva} < 1000 (mm a^{-1}) rarely arises and indicates a transition zone into tropical areas.

Considering the influence of soil properties on R_{gw}, topsoil maximum water storage capacity exhibits the strongest correlation (r_s = 0.56, Fig. 5c). The larger the topsoil water storage capacity, the more water can be stored, contributing to subsoil infiltration and groundwater recharge.

In addition, the weak correlation between topsoil and subsoil saturated hydraulic conductivity and R_{gw} (Fig. 5d and 5e) can be attributed to the collective influence of topsoil and subsoil properties on R_{gw}. The negative correlation between these two soil properties and R_{gw} also indicates that soil hydraulic conductivity tends to be higher in arid areas with less rainfall and accordingly lower recharge (r_s = -0.76 and r_s = -0.74 are correlations between precipitation and topsoil and subsoil saturated hydraulic conductivity, respectively, Supplementary Fig. SF1).

3.4. Long-term temporal distribution of recharge

The temporal distribution of recharge in river basins spanning from 2001 to 2020 was evaluated using linear regression analysis. The R_{gw} trend, herein denoted as the slope of the linear regression line, quantifies the annual change in R_{gw} over the study period. It also serves as an

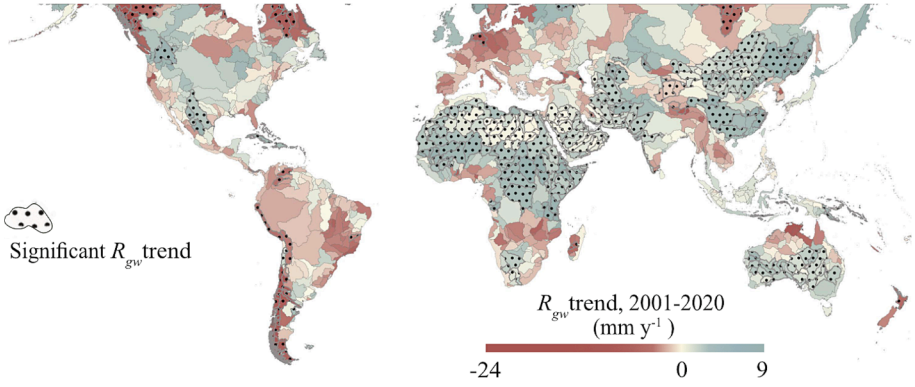

Fig. 6. Average annual rain-fed groundwater recharge R_{gw} trend per basin (2001–2020) with indication of statistically significant trend (p-value < 0.05).

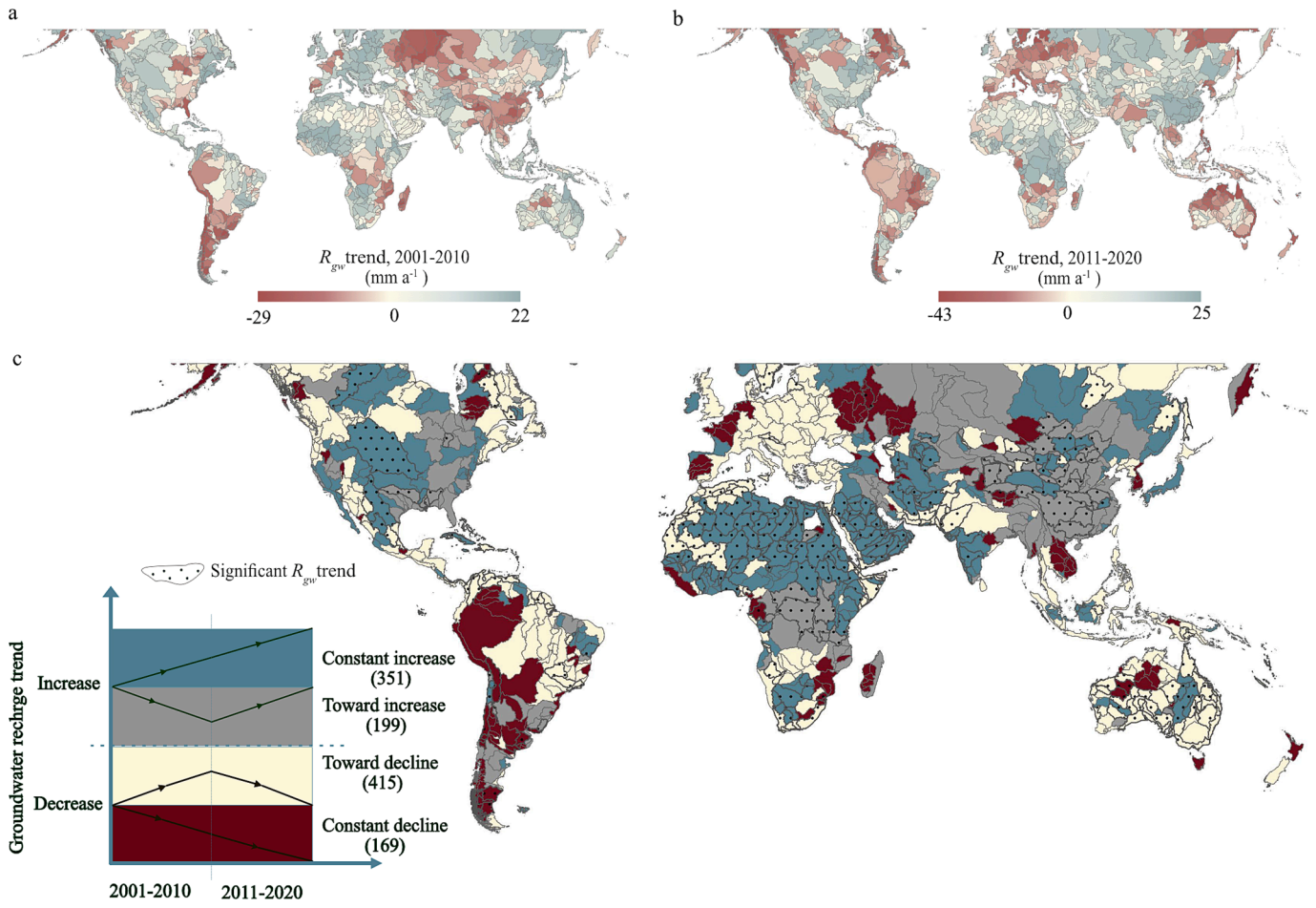

Fig. 8. Average annual rain-fed groundwater recharge R_{gw} trend per river basin for two decades (a) 2001–2010, and (b) 2011–2020; and (c) the two decades trends are compared, considering two sorts of trends, increasing and decreasing (numbers in parentheses indicate the number of river basins in each category).

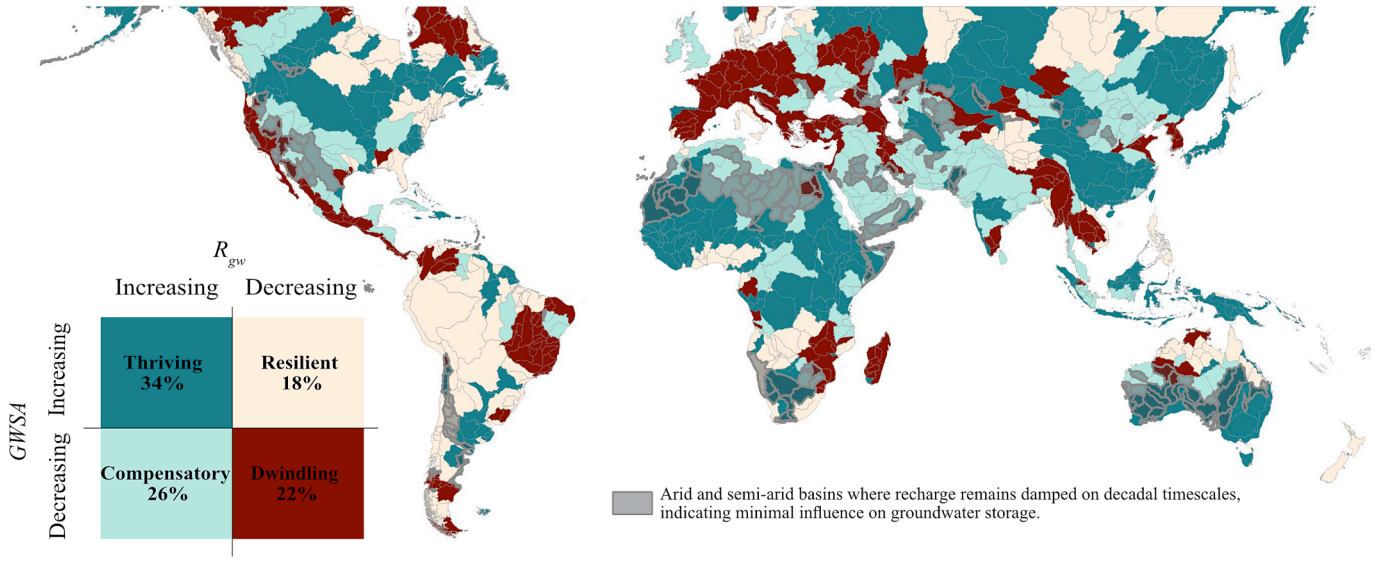

Fig. 9. Comparison of Groundwater Storage Anomaly (GWSA) and rain-fed groundwater recharge R_{gw} dynamics, highlighting basins where groundwater recharge is damped and has minimal influence on groundwater storage, as a function of damping depth calculated by Moeck et al. (2024). The values indicate the percentages of the basins in each category. The four categories describing the role of groundwater recharge in groundwater storage are: Thriving basins, where both recharge and storage are increasing; Compensatory basins, where recharge is increasing and storage is sinking; Resilient basins, which are resilient to recharge reduction; and Dwindling basins, where drying recharge exacerbates storage loss, and are considered as climatic hotspots for groundwater sustainability.

indicator of climatic variability and its influence on groundwater conditions. Linear regression results disclosed that the R_{gw} trend across basins varied from −24 mm a^{-1} to 9 mm a^{-1} over the 20-year modeling period (Fig. 6). On average, global recharge demonstrated an annual increase of 0.2 mm a^{-1}. This variation, when normalized to the basins' long-term average R_{gw}, ranged from a 12 % decline to a 28 % increase annually (for basins with very small annual recharge).

In 40 % of the river basins, R_{gw} showed a declining trend, notably throughout South America and Europe, with additional scattered basins in northern Australia, Myanmar, China, Thailand, Cambodia, Vietnam, Kyrgyzstan, and Russia. Conversely, wetting trends were observed in the Sahara Desert, the Sahel region, Saudi Arabia, and several basins in Iran, Pakistan, China, and Australia. Figure SF2 shows the contribution of the input datasets to the recharge trend, including rainfall, snowmelt, and total evapotranspiration.

Moreover, we studied which basins exhibited statistically significant wetting or drying trends, based on a significance level of p-value < 0.05. Our results revealed that 33 % of the basins displayed significant trends, of which 82 % were characterized by wetting trends, as shown in Fig. 6.

3.5. Temporal variability of recharge

To examine recent changes in recharge, the modeling period was divided into two intervals, 2001–2010 and 2011–2020. The average recharge for the first and second decades was calculated to be 173 and 178 mm a^{-1} per grid unit, respectively (Fig. 7). While the average R_{gw} increased slightly in the second decade, the recharge trend changed from an average increase of 1.3 mm a^{-1} per unit area, to a decrease of −0.8 mm a^{-1} in the second decade.

The frequency of R_{gw} trends in river basins for both decades was calculated and compared in Fig. 7. The R_{gw} trend from 2001 to 2010 revealed an increase in recharge in 67 % of the world's basins, while from 2011 to 2020, this increasing trend was observed in 48 % of the basins.

Upon comparing the R_{gw} trends in each basin over these two decades, it is evident that the recharge trend remained increasing for 30 % of the basins and decreasing for 15 % of the basins in both decades. However, in 35 % of all the basins, the R_{gw} trend shifted towards a decline in the second decade (Fig. 8).

While a 10-year period is too short to evaluate the impact of climate change on recharge, it is observed that climate variability in the last decade has led to more frequent instances of R_{gw} drying worldwide. About 50 % of the world's population (3.6 billion people) inhabit basins where the groundwater recharge (R_{gw}) has either constantly decreased over the past 20 years or has shifted towards a decline in the last 10 years.

While this study does not project recharge trends into the future, past changes are consistent with projected recharge trends in the existing literature (Reinecke et al., 2021) in the majority of river basins. For instance, a drying trend is projected for northeast Brazil, southern Chile, southern Europe, and east China, while an increasing trend is anticipated for east Africa and India. Despite the inherent uncertainty in recharge projections, it is evident that these projected trends are already emerging for the majority of global basins.

3.6. Recharge contribution to storage variability

The comparison between the trends of groundwater storage anomaly and R_{gw} showed a consistent pattern in the majority of the world's basins. In 34 % of the basins, an increase in recharge coincided with an increase in storage, indicating a wetting trend (Fig. 9). These basins present the thriving role of groundwater recharge on groundwater resources and are mainly prominent in regions like Sub-Saharan Africa, southern Australia, and North America. Further studies are needed to evaluate whether this wetting recharge trend can provide opportunities to enhance groundwater usage, especially in Sub-Saharan Africa, where currently only 5 % of irrigated areas utilize groundwater (United Nations, 2022).

Conversely, in 22 % of the basins, both decreases in recharge and storage were observed, indicating a drying trend. It is challenging to discern the predominant factor of sinking storage in these cases. However, the dwindling recharge exacerbates storage loss, especially in comparison to basins with increasing recharge, which can mitigate human-induced impacts. This co-occurrence is considered here to identify climatic hotspots for groundwater sustainability, affecting 1.7 billion inhabitants.

In 44 % of the basins, the dynamics of recharge did not align with changes in storage. It is expected that an increase in recharge, as the primary natural factor replenishing groundwater storage, would lead to an increase in storage. However, in 26 % of the basins experiencing an increase in recharge, a corresponding increase in storage is not observed. This suggests that direct anthropogenic drivers, such as overexploitation, are the major factors causing storage losses. These basins are home to 2.6 billion people. This phenomenon is particularly evident in regions like the Indo-Gangetic Plain and northwestern India, where intensive irrigation practices have led to overexploited groundwater resources and high depletion rates (Dangar et al., 2021; Mishra et al., 2018). Similar situations are observed in countries such as Saudi Arabia, Iran, Iraq and parts of western China. In these basins, the slight increase in recharge has not been able to compensate for the anthropogenic impact and has led to a reduction in storage.

In the remaining basins, a decrease in recharge was associated with an increase in storage. These basins present to be resilient to the reduced recharge, which can be attributed to reductions in groundwater abstraction or the impacts of other recharge sources. For instance, the implementation of Integrated Water Resources Management (IWRM) strategies has been shown to reduce the vulnerability of freshwater resources (Huggins et al., 2022).

Incorporating annual and decadal damping depths (Moeck et al., 2024) into our assessment shows that in approximately 60 % of the river basins within our study domain, the annual recharge cycle is transient, meaning that annual variability in recharge should have a noticeable impact on groundwater storage. However, in 35 % of the river basins, primarily located in arid and semi-arid regions with deep groundwater tables, the recharge is steady over a 10-year timescale. In these regions, recharge variability over decadal periods should have minimal impact on groundwater storage, and the timeframe of this study may be too short to see changes. Longer-term assessments are necessary in these areas to accurately capture the influence of recharge variation on groundwater storage. This will become increasingly possible in the future, as satellite products cover longer periods.

3.7. Limitations

The presented analysis of the spatiotemporal distribution of global groundwater recharge is based on the development of a grid-based water balance model. However, this approach is associated with limitations and uncertainties.

This study focuses solely on rain-fed recharge, not accounting for focused recharge from surface water. Based on evaluations using the WaterGAP2.2e model (Müller Schmied, 2024; Gosling et al., 2024), focused recharge contributes, on average, about 10 % of the total recharge in river basins. Ignoring focused recharge can lead to an underestimation of total groundwater recharge, particularly in basins with losing streams, where groundwater-surface water interactions are critical (Condon et al., 2021; Döll and Fiedler, 2008).

Recharge estimates in permafrost regions are subject to additional uncertainties. The GGR model does not account for soil seasonal freezing or permafrost processes, which may result in an underestimation of recharge during warmer seasons and an overestimation during colder seasons in these zones (Diak et al., 2023). Additionally, the model's ability to capture macropore effects, such as those found in karstic

regions, is limited by the soil and aquifer property datasets used. The absence of specific differentiation for karstic areas may lead to an underestimation of recharge in these regions.

The assessment of the impacts of teleconnections, vadose zone processes, and recharge variability on groundwater storage is constrained by the time scale of this study. While annual to decadal phenomena can be evaluated, longer-term climate cycles (e.g., 15–30 years) are beyond the scope of the current analysis. Moreover, the model's ability to capture the impact of recharge variability in areas with deep groundwater tables, such as arid regions, is limited.

Finally, the GGR model, like other GHMs, is subject to uncertainties arising from input meteorological and soil property data. The overestimation of recharge due to the use of land cover data that fails to accurately represent vegetation types (Wan et al., 2024) underscores how GHMs could be significantly improved with more precise input data. While these limitations are inherent to the study and may impact the total estimated recharge values, we expect they should not significantly alter the observed recharge trends over time in each region.

Furthermore, the limitations of available global groundwater recharge observation datasets underscore the need for the development of more comprehensive datasets for systematic validation of global models. Improvements in observational data will support a deeper understanding of global groundwater recharge dynamics and enhance water resource management strategies.

4. Conclusion

We assessed the spatial and temporal patterns of global rain-fed groundwater recharge over the past two decades (2001–2020) to understand the influence of climate variability and change on groundwater recharge across global river basins. To achieve this, we developed the Global Groundwater Rain-fed Recharge (GGR) model—a three-layer, transient water balance model. The GGR model integrates global meteorological datasets and soil properties, operating daily at a spatial resolution of 0.1° for the period from 2001 to 2020.

The modeled average global groundwater recharge between 2001 and 2020 is 176 mm a^{-1}, closely following the global precipitation pattern. Groundwater recharge rates are lowest in arid regions, while basins located in the tropics and northern mid-latitudes have the highest groundwater recharge rates. Over the 20-year period, groundwater recharge has varied across global river basins from −24 mm a^{-1} to 9 mm a^{-1}.

The recent variability of groundwater recharge from 2011 to 2020 was also examined and compared with the recharge changes over the 2001–2010 period. It was observed that while the average recharge increased from 173 to 178 mm a^{-1} in the second decade, its temporal trend showed a decline from 1.3 to −0.8 mm a^{-1}. In 50 % of the river basins, inhabited by 52 % of the global population (3.6 billion people), groundwater recharge has either constantly declined during the study period or shifted towards a decreasing trend in the second decade.

The combined analysis of rain-fed groundwater recharge and the Global Gravity-based Groundwater Product (G3P) helps distinguish the role of groundwater recharge in groundwater storage dynamics. In 26 % of the world's basins, home to 2.6 billion people, storage loss is likely attributable to anthropogenic factors such as over-exploitation rather than climatic variability. However, 1.7 billion people live in the 22 % of basins where groundwater recharge reduction coincides with declining groundwater storage. These basins were identified as hotspots, where dwindling groundwater recharge can exacerbate groundwater storage loss and stress groundwater resources.

5. Code availability

The source code of GGR model is available under the GNU General Public License v3.0 at Zenodo https://doi.org/10.5281/zenodo.13225038 (Nazari, 2024).

Declaration of Generative AI and AI-Assisted Technologies in the Writing Process

During the preparation of this work, the authors used ChatGPT, an AI language model developed by OpenAI, in order to improve the clarity of the writing. After using this tool, the authors reviewed and edited the content as needed and take full responsibility for the content of the published article.

CRediT authorship contribution statement

S. Nazari: Writing – original draft, Visualization, Software, Methodology, Formal analysis, Data curation, Conceptualization. **I.L. Kruse:** Writing – review & editing, Methodology, Conceptualization. **N. Moosdorf:** Writing – review & editing, Supervision, Methodology, Conceptualization.

Declaration of competing interest

The authors declare that they have no known competing financial interests or personal relationships that could have appeared to influence the work reported in this paper.

Acknowledgments

The authors express their gratitude to the four anonymous reviewers for their constructive comments, which greatly enhanced the quality of this manuscript. We also extend our thanks to Dr. Inge de Graaf, Dr. Wouter Berghuijs, and Dr. Ehsan Sharifi for providing invaluable data that supported this research. Furthermore, we are grateful for the guidance and insightful discussions offered by Dr. Robert Reinecke and Dr. Tobias Stacke.

Appendix A. Supplementary data

Supplementary data to this article can be found online at https://doi.org/10.1016/j.jhydrol.2024.132490.

Data availability

All the input datasets used to develop the GGR model in this study are available through the sources cited. The main output of this study, grid-based annual global rain-fed groundwater recharge from 2001 to 2020, is available at PANGEA Database https://doi.pangaea.de/10.1594/PANGAEA.957447 (Nazari et al., 2024).

References

Alley, W.M., Healy, R.W., LaBaugh, J.W., Reilly, T.E., 2002. Flow and storage in groundwater systems. Science 296 (5575), 1985–1990. https://doi.org/10.1126/science.1067123.

Amante, C., Eakins, B., 2009. ETOPO1 1 arc-minute global relief model: procedures, data sources and analysis. NOAA technical memorandum NESDIS NGDC-24. National Geophysical Data Center, NOAA, 10(2009): V5C8276M. Doi: 10.7289/V5C8276M.

Berghuijs, W.R., Luijendijk, E., Moeck, C., van der Velde, Y., Allen, S.T., 2022. Global recharge data set indicates strengthened groundwater connection to surface fluxes. Geophys. Res. Lett. 49 (23), e2022GL099010. https://doi.org/10.1029/2022GL099010.

Berghuijs, W.R., Collenteur, R.A., Jasechko, S., Jaramillo, F., Luijendijk, E., Moeck, C., van der Velde, Y., Allen, S.T., 2024. Groundwater recharge is sensitive to changing long-term aridity. Nat. Clim. Change 14, 357–363. https://doi.org/10.1038/s41558-024-01953-z.

[dataset] Berghuijs, W.R., 2022. Global groundwater recharge estimates (Version 2), Zenodo. Doi: 10.5281/zenodo.7611675.

Bergkamp, G., Cross, K., 2006. Groundwater and ecosystem services: towards their sustainable use, Proceedings of the International Symposium on Groundwater Sustainability (ISGWAS), IUCN – The World Conservation Union, Rue Mauverney 28, 1196 Gland, Switzerland, pp. 177-193.

Bierkens, M.F.P., Sutanudjaja, E.H., Wanders, N., 2021. Large-scale sensitivities of groundwater and surface water to groundwater withdrawal. Hydrol. Earth Syst. Sci. 25 (11), 5859–5878. https://doi.org/10.5194/hess-25-5859-2021.

[dataset] Center for International Earth Science Information Network - CIESIN - Columbia University, 2018. Gridded Population of the World, Version 4 (GPWv4): Population Density, Revision 11, [Dataset]. NASA Socioeconomic Data and Applications Center (SEDAC), Palisades, New York.
Chen, Z., et al., 2017. World Karst Aquifer Map (WHYMAP WOKAM). BGR, IAH, KIT, UNESCO. https://doi.org/10.25928/b2.21_sfkq-r406.
Chen, J., Famiglietti, J.S., Scanlon, B.R., Rodell, M., 2016. Groundwater storage changes: present status from GRACE observations. Remote Sensing and Water Resources 207–227. https://doi.org/10.1007/978-3-319-32449-4_9.
Condon, L.E., Kollet, S., Bierkens, M.F., Fogg, G.E., Maxwell, R.M., Hill, M.C., Fransen, H. J.H., Verhoef, A., Van Loon, A.F., Sulis, M., 2021. Global groundwater modeling and monitoring: Opportunities and challenges. Water Resour. Res. 57 (12), e2020WR029500. https://doi.org/10.1029/2020WR029500.
Corona, C.R., Gurdak, J.J., Dickinson, J.E., Ferré, T., Maurer, E.P., 2018. Climate variability and vadose zone controls on damping of transient recharge. J. Hydrol. 561, 1094–1104.
Cuthbert, M., Gleeson, T., Moosdorf, N., Befus, K.M., Schneider, A., Hartmann, J., Lehner, B., 2019. Global patterns and dynamics of climate–groundwater interactions. Nat. Clim. Chang. 9 (2), 137–141. https://doi.org/10.1038/s41558-018-0386-4.
Dalin, C., Wada, Y., Kastner, T., Puma, M.J., 2017. Groundwater depletion embedded in international food trade. Nature 543 (7647), 700–704. https://doi.org/10.1038/nature21403.
Dangar, S., Asoka, A., Mishra, V., 2021. Causes and implications of groundwater depletion in India: A review. J. Hydrol. 596, 126103. https://doi.org/10.1016/j.jhydrol.2021.126103.
de Graaf, I.E.M., Sutanudjaja, E.H., van Beek, L.P.H., Bierkens, M.F.P., 2015. A high-resolution global-scale groundwater model. Hydrol. Earth Syst. Sci. 19 (2), 823–837. https://doi.org/10.5194/hess-19-823-2015.
de Graaf, I.E.M., van Beek, L.P.H., Gleeson, T., Moosdorf, N., Schmitz, O., Sutanudjaja, E. H., Bierkens, M.F.P., 2017. A global-scale two-layer transient groundwater model: Development and application to groundwater depletion. Adv. Water Resour. 102, 53–67. https://doi.org/10.1016/j.advwatres.2017.01.011.
de Graaf, I.E.M., Gleeson, T., van Beek, L.P.H., Sutanudjaja, E.H., Bierkens, M.F.P., 2019. Environmental flow limits to global groundwater pumping. Nature 574 (7776), 90–94. https://doi.org/10.1038/s41586-019-1594-4.
De Vries, J.J., Simmers, I., 2002. Groundwater recharge: an overview of processes and challenges. Hydrgeol. J. 10, 5–17. https://doi.org/10.1007/s10040-001-0171-7.
Delleur, J.W., 2006. The handbook of groundwater engineering. CRC Press.
Diak, M., Böttcher, M.E., Ehlert von Ahn, C.M., Hong, W.-L., Kędra, M., Kotwicki, L., Koziorowska-Makuch, K., Kuliński, K., Lepland, A., Makuch, P., 2023. Permafrost and groundwater interaction: current state and future perspective. Front. Earth Sci. 11, 1254309. https://doi.org/10.3389/feart.2023.1254309.
Dickinson, J.E., Ferré, T., Bakker, M., Crompton, B., 2014. A screening tool for delineating subregions of steady recharge within groundwater models. Vadose Zone J. 13 (6).
Döll, P., Fiedler, K., 2008. Global-scale modeling of groundwater recharge. Hydrology and Earth System Sciences 12 (3), 863–885. https://doi.org/10.5194/hess-12-863-2008.
Döll, P., Hoffmann-Dobrev, H., Portmann, F.T., Siebert, S., Eicker, A., Rodell, M., Strassberg, G., Scanlon, B., 2012. Impact of water withdrawals from groundwater and surface water on continental water storage variations. Journal of Geodynamics 59, 143–156. https://doi.org/10.1016/j.jog.2011.05.001.
Döll, P., Fritsche, M., Eicker, A., Schmied, H.M., 2014a. Seasonal water storage variations as impacted by water abstractions: comparing the output of a global hydrological model with GRACE and GPS observations. Surv. Geophys. 35 (6), 1311–1331. https://doi.org/10.1007/s10712-014-9282-2.
Döll, P., Mueller Schmied, H., Schuh, C., Portmann, F.T., Eicker, A., 2014b. Global-scale assessment of groundwater depletion and related groundwater abstractions: combining hydrological modeling with information from well observations and GRACE satellites. Water Resour. Res. 50 (7), 5698–5720. https://doi.org/10.1002/2014WR015595.
ECMWF, 2016. IFS Documentation CY41R2 - Part IV: Physical Processes, IFS Documentation CY41R2. Doi: 10.21957/tr5rv27xu.
Famiglietti, J.S., 2014. The global groundwater crisis. Nat. Clim. Chang. 4 (11), 945–948. https://doi.org/10.1038/nclimate2425.
Fleming, S.W., Quilty, E.J., 2006. Aquifer responses to el Niño–Southern oscillation, southwest British Columbia. Groundwater 44 (4), 595–599. https://doi.org/10.1111/j.1745-6584.2006.00187.x.
Gleeson, T., Moosdorf, N., Hartmann, J., Van Beek, L., 2014. A glimpse beneath earth's surface: GLobal HYdrogeology MaPS (GLHYMPS) of permeability and porosity. Geophys. Res. Lett. 41 (11), 3891–3898. https://doi.org/10.1002/2014GL059856.
Gleeson, T., Cuthbert, M., Ferguson, G., Perrone, D., 2020. Global groundwater sustainability, resources, and systems in the Anthropocene. Annu. Rev. Earth Planet. Sci. 48, 431–463. https://doi.org/10.1146/annurev-earth-071719-055251.
Gong, C., Cook, P.G., Therrien, R., Wang, W., Brunner, P., 2023. On groundwater recharge in variably saturated subsurface flow models. Water Resour. Res. 59 (9). https://doi.org/10.1029/2023WR034920.
[dataset] Gosling, S.N., Schmied, H.M., Burek, P., Guillaumot, L., Hanasaki, N., Kou-Giesbrecht, S., Otta, K., Sahu, R.-K., Satoh, Y., Schewe, J., 2024. ISIMIP3b Simulation Data from the Global Water Sector (v1.2). ISIMIP Repository. Doi: 10.48364/ISIMIP.230418.2.
[dataset] Simon N. Gosling et al., 2024. ISIMIP3a Simulation Data from the Global Water Sector (v1.3). In: Repository, I. (Ed.). Doi: 10.48364/ISIMIP.398165.3.
Gruber, S., 2012. Derivation and analysis of a high-resolution estimate of global permafrost zonation. Cryosphere 6 (1), 221–233. https://doi.org/10.5194/tc-6-221-2012.
Güntner, A., et al., 2023. Global Gravity-based Groundwater Product (G3P). V. 1.11., GFZ Data Services. Doi: 10.5880/G3P.2023.001.
Hagemann, S., Gates, L.D., 2003. Improving a subgrid runoff parameterization scheme for climate models by the use of high resolution data derived from satellite observations. Clim. Dyn. 21 (3), 349–359. https://doi.org/10.1007/s00382-003-0349-x.
[dataset] Hengl, T., Mendes de Jesus, J., Heuvelink, G.B., Ruiperez Gonzalez, M., Kilibarda, M., Blagotić, A., Shangguan, W., Wright, M.N., Geng, X., Bauer-Marschallinger, B., 2017. SoilGrids250m: Global gridded soil information based on machine learning. PLoS one, 12(2), e0169748.
[dataset] Huffman, G.J., E.F. Stocker, D.T. Bolvin, E.J. Nelkin, Jackson Tan 2019. GPM IMERG Final Precipitation L3 1 day 0.1 degree x 0.1 degree V06, Edited by Andrey Savtchenko, Greenbelt, MD, Goddard Earth Sciences Data and Information Services Center (GES DISC), Doi: 10.5067/GPM/IMERGDF/DAY/06.
Hajati, M.C., Sutanudjaja, E., Moosdorf, N., 2019. Quantifying Regional Fresh Submarine Groundwater Discharge With the Lumped Modeling Approach CoCa-RFSGD. Water Res. Res. 55 (7), 5321–5341. https://doi.org/10.1029/2018WR024248.
Huggins, X., Gleeson, T., Kummu, M., Zipper, S.C., Wada, Y., Troy, T.J., Famiglietti, J.S., 2022. Hotspots for social and ecological impacts from freshwater stress and storage loss. Nat. Commun. 13 (1), 1–11. https://doi.org/10.1038/s41467-022-28029-w.
Humphrey, V., Rodell, M., Eicker, A., 2023. Using satellite-based terrestrial water storage data: a review. Surv. Geophys. 1–29. https://doi.org/10.1007/s10712-022-09754-9.
Jung, H., Saynisch-Wagner, J., Schulz, S., 2024. Can eXplainable AI offer a new perspective for groundwater recharge estimation?—Global-scale modeling using neural network. Water Resour. Res. 60 (4), e2023WR036360.
Kløve, B., Ala-Aho, P., Bertrand, G., Boukalova, Z., Ertürk, A., Goldscheider, N., Ilmonen, J., Karakaya, N., Kupfersberger, H., Kværner, J., 2011. Groundwater dependent ecosystems. Part I: Hydroecological status and trends. Environ Sci Policy 14 (7), 770–781. https://doi.org/10.1016/j.envsci.2011.04.002.
Kundzewicz, Z.W., Mata, L.J., Arnell, N., Doll, P., Kabat, P., Jimenez, B., Miller, K., Oki, T., Zekai, S., Shiklomanov, I., 2007. In: Freshwater Resources and Their Management. Cambridge University Press, pp. 173–210.
Kuss, A.J.M., Gurdak, J.J., 2014. Groundwater level response in US principal aquifers to ENSO, NAO, PDO, and AMO. J. Hydrol. 519, 1939–1952. https://doi.org/10.1016/j.jhydrol.2014.09.069.
Lehner, B., Grill, G., 2013. Global river hydrography and network routing: baseline data and new approaches to study the world's large river systems. Hydrol. Process. 27 (15), 2171–2186. https://doi.org/10.1002/hyp.9740.
Li, Z., Tang, G., Hong, Z., Chen, M., Gao, S., Kirstetter, P., Gourley, J.J., Wen, Y., Yami, T., Nabih, S., 2021. Two-decades of GPM IMERG early and final run products intercomparison: Similarity and difference in climatology, rates, and extremes. J. Hydrol. 594, 125975. https://doi.org/10.1016/j.jhydrol.2021.125975.
Mishra, V., Asoka, A., Vatta, K., Lall, U., 2018. Groundwater depletion and associated CO2 emissions in India. Earth's Future 6 (12), 1672–1681. https://doi.org/10.1029/2018EF000939.
Moeck, C., Collenteur, R.A., Berghuijs, W.R., Luijendijk, E., Gurdak, J.J., 2024. A global assessment of groundwater recharge response to infiltration variability at monthly to decadal timescales. Water Resour. Res. 60 (6), e2023WR035828. https://doi.org/10.1029/2023WR035828.
Moeck, C., Grech-Cumbo, N., P., J., B., A., , Gurdak, J.J., Berg, M., Schirmer, M., 2020a. Data for: A global-scale dataset of direct natural groundwater recharge rates: A review of variables, processes and relationships, Eawag: Swiss Federal Institute of Aquatic Science and Technology. Doi: org/10.25678/0001NG.
Moeck, C., Grech-Cumbo, N., Podgorski, J., Bretzler, A., Gurdak, J.J., Berg, M., Schirmer, M., 2020b. A global-scale dataset of direct natural groundwater recharge rates: a review of variables, processes and relationships. Sci. Total Environ. 717, 137042. https://doi.org/10.1016/j.scitotenv.2020.137042.
Mohan, C., Gleeson, T., Forstner, T., Famiglietti, J.S., de Graaf, I., 2023. Quantifying Groundwater's Contribution to Regional Environmental-Flows in Diverse Hydrologic Landscapes. Water Resour. Res. 59 (6), e2022WR033153. https://doi.org/10.1029/2022WR033153.
Mualem, Y., 1976. A new model for predicting the hydraulic conductivity of unsaturated porous media. Water Resour. Res. 12 (3), 513–522. https://doi.org/10.1029/WR012i003p00513.
Müller Schmied, et al., 2024. The global water resources and use model WaterGAP v2.2e: description and evaluation of modifications and new features. Geosci. Model Dev. 17 (23), 8817–8852. https://doi.org/10.5194/gmd-17-8817-2024.
Müller Schmied, H., Cáceres, D., Eisner, S., Flörke, M., Herbert, C., Niemann, C., Peiris, T. A., Popat, E., Portmann, F.T., Reinecke, R., 2021. The global water resources and use model WaterGAP v2. 2d: Model description and evaluation. Geosci. Model Dev. 14 (2), 1037–1079. https://doi.org/10.5194/gmd-14-1037-2021.
[dataset] Hengl, T., Mendes de Jesus, J., Heuvelink, G.B., Ruiperez Gonzalez, M., Kilibarda, M., Blagotić, A., Shangguan, W., Wright, M.N., Geng, X., Bauer-Marschallinger, B., 2017. SoilGrids250m: Global gridded soil information based on machine learning. PLoS one, 12(2): e0169748. Muñoz Sabater, J., 2019. ERA5-Land hourly data from 1950 to present. , Copernicus Climate Change Service (C3S) Climate Data Store (CDS) Doi: 10.24381/cds.e2161bac.
[dataset] Nazari, S., Kruse, I.L., Moosdorf, N., 2024. Grid-based rain-fed annual global groundwater recharge. PANGAEA. Doi: 10.1594/PANGAEA.957447.
Nazari, S., 2024. Source code for the Global Groundwater rain-fed Recharge (GGR) model (v1.0). Zenodo. https://doi.org/10.5281/zenodo.13225038.
Reinecke, R., Müller Schmied, H., Trautmann, T., Andersen, L.S., Burek, P., Flörke, M., Gosling, S.N., Grillakis, M., Hanasaki, N., Koutroulis, A., 2021. Uncertainty of

simulated groundwater recharge at different global warming levels: a global-scale multi-model ensemble study. Hydrol. Earth Syst. Sci. 25 (2), 787–810. https://doi.org/10.5194/hess-25-787-2021.

Rodell, M., Velicogna, I., Famiglietti, J.S., 2009. Satellite-based estimates of groundwater depletion in India. Nature 460 (7258), 999–1002. https://doi.org/10.1038/nature08238.

Rodell, M., Famiglietti, J.S., Wiese, D.N., Reager, J., Beaudoing, H.K., Landerer, F.W., Lo, M.-H., 2018. Emerging trends in global freshwater availability. Nature 557 (7707), 651–659. https://doi.org/10.1038/s41586-018-0123-1.

Rust, W., Holman, I., Bloomfield, J., Cuthbert, M., Corstanje, R., 2019. Understanding the potential of climate teleconnections to project future groundwater drought. Hydrol. Earth Syst. Sci. 23 (8), 3233–3245. https://doi.org/10.5194/hess-23-3233-2019.

Scanlon, B.R., Reedy, R.C., Stonestrom, D.A., Prudic, D.E., Dennehy, K.F., 2005. Impact of land use and land cover change on groundwater recharge and quality in the southwestern US. Glob. Chang. Biol. 11 (10), 1577–1593. https://doi.org/10.1111/j.1365-2486.2005.01026.x.

Sharifi, E., Güntner, A., 2022. The Global Gravity-based Groundwater Product (G3P): first results, EGU General Assembly Conference Abstracts, pp. EGU22-1659. Doi: 10.5194/egusphere-egu22-1659.

Sharifi, E., Güntner, A., Haas, J., Dorigo, W., Jäggi, A., Ruz Vargas, C., 2023. G3P: A global data set of groundwater storage variations based on satellite gravimetry, EGU General Assembly Conference Abstracts, pp. EGU-10289. Doi: 10.5194/egusphere-egu22-1659.

[dataset] Simons, G., Koster, R., Droogers, P., 2020. HiHydroSoil v2. 0-High Resolution Soil Maps of Global Hydraulic Properties. FutureWater report 134, Wageningen, The Netherlands.

Small, E.E., 2005. Climatic controls on diffuse groundwater recharge in semiarid environments of the southwestern United States. Water Resour. Res. 41 (4). https://doi.org/10.1029/2004WR003193.

[dataset] Stacke, T., Hagemann, S., 2021. Land surface parameter fields at 0.5deg resolution for use with the HydroPy model (1.0.0) Zenodo. Doi: 10.5281/zenodo.4541391-28.

United Nations, 2022. The United Nations World Water Development Report 2022. Groundwater: Making the invisible visible. UNESCO, Paris.

Van Genuchten, M.T., 1980. A closed-form equation for predicting the hydraulic conductivity of unsaturated soils. Soil Sci. Soc. Am. J. 44 (5), 892–898. https://doi.org/10.2136/sssaj1980.03615995004400050002x.

Vinueza, A.U., Vargas, C.R., Contreras, S., Imran, T., 2023. G3P Evaluation Report, Deliverable 4.2. Technical Report. Global Gravity-based Groundwater Product (G3P) Project.

Wada, Y., 2016. Modeling groundwater depletion at regional and global scales: present state and future prospects. Surv. Geophys. 37 (2), 419–451. https://doi.org/10.1007/s10712-015-9347-x.

Wada, Y., Van Beek, L.P., Van Kempen, C.M., Reckman, J.W., Vasak, S., Bierkens, M.F.P., 2010. Sup-Global depletion of groundwater resources. Geophys. Res. Lett. 37 (20). https://doi.org/10.1029/2010GL044571.

Wada, Y., Wisser, D., Bierkens, M.F.P., 2014. Global modeling of withdrawal, allocation and consumptive use of surface water and groundwater resources. Earth Syst. Dyn. 5 (1), 15–40. https://doi.org/10.5194/esd-5-15-2014.

Wan, W., Döll, P., Müller Schmied, H., 2024. Global-scale groundwater recharge modeling is improved by tuning against ground-based estimates for karst and non-karst areas. Water Resour. Res. 60 (3), e2023WR036182. https://doi.org/10.1029/2023WR036182.

Wieder, W., 2014. Regridded Harmonized World Soil Database v1.2. ORNL Distributed Active Archive Center. Doi: 10.3334/ORNLDAAC/1247.

Wiese, D.N., Yuan, D.-N., Boening, C., Landerer, F.W., M., W.M., 2016. JPL GRACE Mascon Ocean, Ice, and Hydrology Equivalent Water Height RL05M.1 CRI Filtered Version 2. In: Ver. 2. PO.DAAC, C., USA. (Ed.). Doi: 10.5067/TEMSC-2LCR5.